coatings

MDPI

Article

Dicalcium Phosphate Coated with Graphene Synergistically Increases Osteogenic Differentiation *In Vitro*

Jun Jae Lee [1,†], Yong Cheol Shin [2,†], Su-Jin Song [3], Jae Min Cha [4], Suck Won Hong [3], Young-Jun Lim [1], Seung Jo Jeong [5], Dong-Wook Han [3,*] and Bongju Kim [6,*]

1 Department of Prosthodontics, Dental Research Institute, School of Dentistry, Seoul National University, Seoul 03080, Korea; jazzyguts@gmail.com (J.J.L.); limdds@snu.ac.kr (Y.-J.L.)
2 Research Center for Energy Convergence Technology, Pusan National University, Busan 46241, Korea; choel15@naver.com
3 Department of Cogno-Mechatronics Engineering, College of Nanoscience & Nanotechnology, Pusan National University, Busan 46241, Korea; songsj86@gmail.com (S.-J.S.); swhong@pusan.ac.kr (S.W.H.)
4 Medical Device Research Center, Samsung Medical Center, Seoul 06351, Korea; jaemin.cha@samsung.com
5 GS Medical Co., Ltd., Cheongju-si, Chungcheongbuk-do 28161, Korea; eric.jeong@gsmedi.com
6 Dental Life Science Research Institute & Clinical Translational Research Center for Dental Science, Seoul National University Dental Hospital, Seoul 03080, Korea
* Correspondence: nanohan@pusan.ac.kr (D.-W.H.); bjkim016@gmail.com (B.K.); Tel.: +82-51-510-7725 (D.-W.H.); +82-2-2072-4455 (B.K.)
† These authors contributed equally to this work.

Academic Editor: Mazeyar Parvinzadeh Gashti
Received: 8 November 2017; Accepted: 26 December 2017; Published: 28 December 2017

Abstract: In recent years, graphene and its derivatives have attracted much interest in various fields, including biomedical applications. In particular, increasing attention has been paid to the effects of reduced graphene oxide (rGO) on cellular behaviors. On the other hand, dicalcium phosphate (DCP) has been widely used in dental and pharmaceutical fields. In this study, DCP composites coated with rGO (DCP-rGO composites) were prepared at various concentration ratios (DCP to rGO concentration ratios of 5:2.5, 5:5, and 5:10 μg/mL, respectively), and their physicochemical properties were characterized. In addition, the effects of DCP-rGO hybrid composites on MC3T3-E1 preosteoblasts were investigated. It was found that the DCP-rGO composites had an irregular granule-like structure with a diameter in the range order of the micrometer, and were found to be partially covered and interconnected with a network of rGO. The zeta potential analysis showed that although both DCP microparticles and rGO sheets had negative surface charge, the DCP-rGO composites could be successfully formed by the unique structural properties of rGO. In addition, it was demonstrated that the DCP-rGO composites significantly increased alkaline phosphatase activity and extracellular calcium deposition, indicating that the DCP-rGO hybrid composites can accelerate the osteogenic differentiation by the synergistic effects of rGO and DCP. Therefore, in conclusion, it is suggested that the DCP-rGO hybrid composites can be potent factors in accelerating the bone tissue regeneration.

Keywords: reduced graphene oxide; dicalcium phosphate; hybrid composite; MC3T3-E1 preosteoblast; osteogenic differentiation; bone tissue regeneration

1. Introduction

Bone fracture is the most common traumatic disease, and results in serious health implications [1,2]. Therefore, tremendous efforts have been devoted to repair and regenerate bone

defects. The currently available strategy for repairing bone fracture includes closed reduction, immobilization with external fixation, and bone graft [3–6]. Among these, bone graft has been extensively used because it can be employed for treatment of bone tumor and spinal diseases, as well as bone fracture [6–9]. Although an autologous bone graft is considered as the most ideal material, but it has a significant limitations, such as limited supply, a risk of infection, a loss of function, and hemorrhage [6,10]. Allografts and xenografts can be alternatives, but the risk of immune response, disease transmission, and graft failure has still remained unsolved problems [11,12]. To address these limitations, tissue engineering approaches have been extensively and actively studied to develop novel bone substitutes using various biomaterials [13–17]. A bioceramic is generally believed to be a promising candidate for bone substitutes due to its superior biocompatibility and strength [18–22]. A calcium phosphate material, such as hydroxyapatite, tricalcium phosphate, and biphasic calcium phosphate, is a representative bioceramic, and has been mainly used for bone tissue engineering because it can be readily obtained by sintering, thermal conversion, coating, and other high-temperature process, and it has excellent biocompatibility, osseoconductivity, and mechanical strength [23–25]. A dicalcium phosphate (DCP), one of the well-known calcium phosphates, has been also widely used for a long time in dental and pharmaceutical fields, such as dental abrasive agent, excipient in pharmaceutical dosage form, and dietary supplement [26–31]. In addition, it has been reported that the DCP shows the superior solubility and biocompatibility, as compared with other calcium phosphate materials, such as tricalcium phosphate, hydroxyapatite, and biphasic calcium [32–34]. Hence, it is possible for DCP to provide a large amount of the constituent ions of bone supporting minerals, including Ca^{2+} and PO_4^{3-}, as DCP is dissolved [32,33,35]. When considering that the bone grafts should be readily resorbed as newly ingrown bone tissues are reconstructed, these high bioresorbability and the ability to provide Ca^{2+} and PO_4^{3-} are quite beneficial to accelerate bone tissue regeneration [33,36]. Meanwhile, the intrinsic brittleness, low wear resistance, and low fracture toughness of DCP are often considered as disadvantages [37,38].

On the other hand, graphene and its derivatives have attracted recent attention as novel nanomaterials in a large variety of fields, including biomedical applications, because of their unique physicochemical, thermomechanical, and biological properties [39–42]. In particular, increasing attention has been paid for the effects of reduced graphene oxide (rGO) on cellular behaviors. It has been documented that the rGO can accelerate the differentiation of various types of cells, such as osteoblasts, myoblasts, chondrocytes, and neuronal cells [43–48].

Herein, we prepared hybrid composites that were composed of commercially available DCP microparticles coated with rGO (DCP-rGO composites), and characterized their structural properties by scanning electron microscopy (SEM), Raman spectroscopy, and dynamic light scattering. In addition, we investigated the biocompatibility of DCP-rGO hybrid composites towards MC3T3-E1 mouse preosteoblasts. Moreover, the effects of DCP-rGO composites on osteogenic differentiation of MC3T3-E1 cells were examined to explore their potentials as bone substitute materials for bone tissue regeneration and engineering.

2. Materials and Methods

The DCP-rGO hybrid composites were prepared by physically mixing DCP microparticles (OssCA™, HansBiomed Co., Daejeon, Korea) with rGO sheets. The rGO sheets were obtained by the preparation of GO using the modified Hummers and offeman method, and subsequent reduction process of GO with hydrazine hydrate ($N_2H_4 \cdot H_2O$) at 100 °C for 24 h [38,49,50]. The prepared rGO sheets in deionized water were sonicated for 2 h. The DCP microparticles dispersed in deionized water were physically mixed at DCP to rGO weight ratios of 2:1, 1:1, or 1:2, respectively. The DCP-rGO composites were mechanically agitated using a vortex mixer for 10 min, followed by slow air-drying at room temperature for overnight.

The surface morphology of DCP-rGO composites was observed by SEM (S-800, Hitach, Tokyo, Japan) with a 15 kV acceleration voltage. The surface potential of the DCP-rGO composites in deionized

water was obtained by a Nano Zetasizer™ (Malvern Instruments, Worcestershire, UK) at 25 °C at a pH value of 7.0, and was measured six times for every sample. The Raman spectra of DCP microparticles and DCP-rGO composites were collected using a Micro Raman spectroscope (Ramboss 500i, Dongwoo Optron Co., Ltd., Kwangju, Korea) excited with Ar-ion (514.5 nm) excitation laser at a laser power of 5 mW.

The MC3T3-E1 preosteoblasts, a murine preosteoblastic cell line, were purchased from the American Type Culture Collection (CRL-2593™, Rockville, MD, USA), and routinely cultured in α-Minimum Essential Medium (Sigma-Aldrich Co., Saint Louis, MO, USA) with fetal bovine serum (10%, Sigma-Aldrich Co.) and antibiotic antimycotic solution (1%, containing 10,000 Units of penicillin, 25 μg of amphotericin B and 10 mg of streptomycin per ml, Sigma-Aldrich Co.) at 37 °C in a humid incubator with 5% CO_2. The effects of DCP-rGO composites on the proliferation of MC3T3-E1 preosteoblasts were examined by a cell counting kit-8 assay (CCK-8 assay, Dojindo, Kumamoto, Japan), following the manufacturer's protocol. The number of viable cells was directly proportional with the metabolite products that were generated in the CCK-8 assay [51]. Typically, MC3T3-E1 preosteoblasts were seeded on 24-well tissue culture plates with a density of 5×10^4 cells/mL, and were cultured for 24 h. Subsequently, DCP-rGO hybrid composites were added to the culture media. The DCP-rGO composites having DCP and rGO at concentration ratios of 5:2.5, 5:5, and 5:10 μg/mL were designated as "DCP5-rGO2.5", "DCP5-rGO5", and "DCP5-rGO10", respectively. According to the manufacturer's protocol, a CCK-8 solution was added after the each culture periods of incubation (1, 7, and 14 days), and were incubated for 2 h at 37 °C in the dark. The absorbance values were measured at 450 nm by using a SpectraMax® 340 spectrophotometer (Molecular Devices, Sunnyvale, CA, USA). The cell viability was expressed as the relative percent of the absorbance value in the cells to the optical density value of control groups. The absorbance values of cultures with fresh media were used as the negative control.

To investigate the osteodifferentiation of MC3T3-E1 cells, the alkaline phosphatase (ALP) quantitative assay and alizarin red S (ARS) staining were conducted. For ALP activity assay, we seeded MC3T3-E1 cells in a 24-well tissue culture plate at a concentration of 1×10^4 cells/mL, and incubated with DCP-rGO hybrid composites for 1 to 21 days. The ALP activity was measured by determining the transformation of ρ-nitrophenyl-phosphate to ρ-nitrophenol using ALP colorimetric assay kit (Abcam, Cambridge, MA, USA). The ALP activity was calculated as the ρ-nitrophenol formation (μmol) divided by the reaction time (min) and the volume of sample (mL). The formation of mineralized nodules was detected by ARS staining. Briefly, the cells were cultured with DCP-rGO composites for 1 to 21 days, and then fixed with a 3.7% formaldehyde solution (Sigma-Aldrich Co.) for 10 min. Subsequently, the cells were stained with 40 mM ARS solution (pH = 4.2, Sigma-Aldrich Co.) for 10 min at room temperature, and then imaged using a digital camera and inverted optical microscope (Leica DM IL LED, Leica Microsystems GmbH, Wetzlar, Germany). To quantify the ARS staining, the ARS in stained cells was extracted with a solution containing 20% methanol and 10% acetic acid in deionized water for 15 min at 37 °C. The ARS was quantified by measuring the absorbance at 405 nm using an ELISA reader (SpectraMax 340, Molecular Device Co., Sunnyvale, CA, USA).

All of the variables were tested in the three other independent experiments, which were repeated two times ($n = 6$). All the presented data are expressed as the average ± standard deviation (SD). Prior to statistical analysis, the test of Levene was conducted to analyze data for the homogeneity of variances. After a one-way analysis of variance (SAS Institute Inc., Cary, NC, USA), statistical comparisons were carried out by a Bonferroni test for multiple comparisons. A value of $p < 0.05$ was deemed statistically significant.

3. Results and Discussion

The prepared DCP-rGO hybrid composites were shown in Figure 1. It is clearly showed that the DCP-rGO composites were homogeneously dispersed in deionized water. The surface morphology of DCP microparticles and DCP5-rGO10 hybrid composites were observed by SEM, as shown in Figure 2.

The SEM images showed that both large and small particles were presented in DCP microparticles with an irregular granule-like structure (Figure 2a,b). On the other hand, the DCP was partly covered and interconnected by an rGO network (yellow arrows) (Figure 2c,d). The coated rGO was obviously observed in DCP-rGO hybrid composites by showing its distinctive wrinkled features.

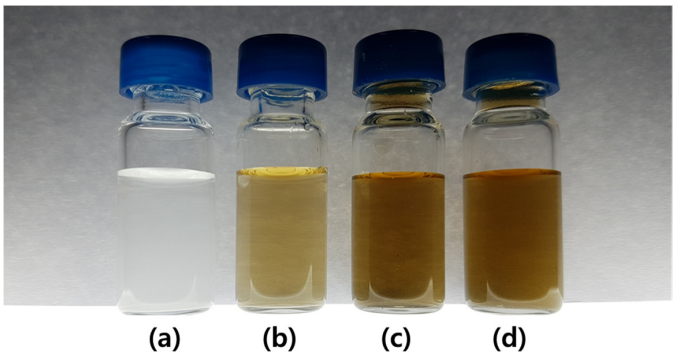

Figure 1. Digital photographs of the (**a**) dicalcium phosphate (DCP) microparticles, (**b**) DCP5-rGO2.5 composites, (**c**) DCP5-rGO5 composites, and (**d**) DCP5-rGO10 composites in deionized water.

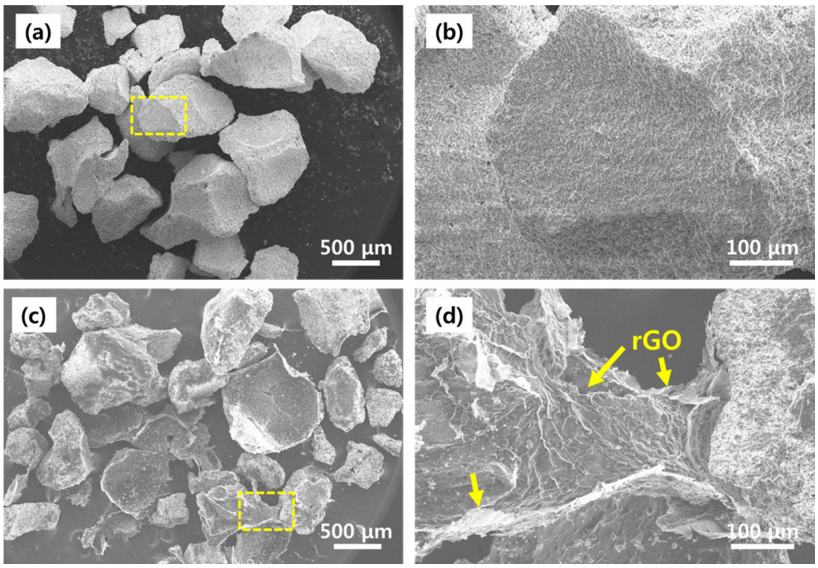

Figure 2. Representative scanning electron microscopy (SEM) images of DCP microparticles and DCP5-rGO10 hybrid composites. (**a**) Low-magnification and (**b**) higher-magnification images of DCP microparticles; (**c**) Low-magnification and (**d**) higher-magnification images of DCP-rGO hybrid composites. Yellow arrows indicate the reduced graphene oxide (rGO). The dashed yellow squares denote the region shown in (**b**,**d**).

To characterize electrochemical properties of DCP-rGO composites, the zeta potential analysis and Raman spectroscopy were performed and the results were presented in Figure 3. The surface charge of DCP microparticles was found to be approximately −15.7 mV, due to the phosphate groups in DCP microparticles (Figure 3a). Meanwhile, the DCP-rGO composites were charged at approximately −29.7 mV. It has been reported that the zeta potentials of rGO vary in the wide range from −25 to −35 mV [52,53]. In general, there are electrostatic repulsion between two materials having negative surface charges. However, previous reports have revealed interesting findings concerning the interactions of graphene nanomaterials with surrounding environments. Even though both GO and polymer (or compounds) have negative surface charge, they can form stable composites [54,55]. This interesting phenomenon can be partly explained by the fact that the negative charges of GO

are mainly existed at its edge sites [54–56]. Therefore, the colloidal particles can be adsorbed on the basal plane of GO sheets. When considering that the negative surface charge density of rGO is lower than that of GO, rGO can also adsorb the colloidal particles of DCP [52]. These interactions are due to the unique structural properties of graphene nanomaterials, which does not appear in other surfactants [54]. Therefore, the DCP-rGO composites could be successfully formed because of the unique structural properties of rGO sheets. In addition, the interfacial and hydrogen bond interactions between the oxygen-containing surface groups of rGO and the hydroxyl groups of DCP microparticles could also participate in the good adhesion between DCP microparticles and rGO [50,57,58]. Figure 3b showed the Raman spectra of DCP microparticles and DCP-rGO composites. The Raman spectroscopy is a highly useful tool for analyzing graphene and its derivatives, since graphene and its derivatives exhibit characteristic bands in their spectra, including D and G bands, at around 1350 and 1600 cm^{-1}, respectively [59–61]. In addition, the intensity ratio of those bands is closely correlated with the nature of graphene materials [62,63]. It has been widely acknowledged that the intensity ratio of D and G bands of rGO is larger than 1 because of the structural defects of sp^2-carbon domains of graphitic structure that is created during reduction process [64,65]. As shown in Figure 3b, the noticeable bands were observed at around 1350 and 1600 cm^{-1} in the spectra of rGO and DCP-rGO composites. Moreover, the intensity ratios of *D* and *G* bands were found to be 1.37 for rGO, 1.05 for DCP5-rGO2.5, 1.09 for DCP5-rGO5, and 1.07 for DCP5-rGO10, respectively. The intensity ratios of *D* and *G* bands of all DCP-rGO composites were found to be higher than 1. Therefore, it is indicated that the rGO sheets were successfully obtained, and the DCP-rGO hybrid composites were successfully prepared.

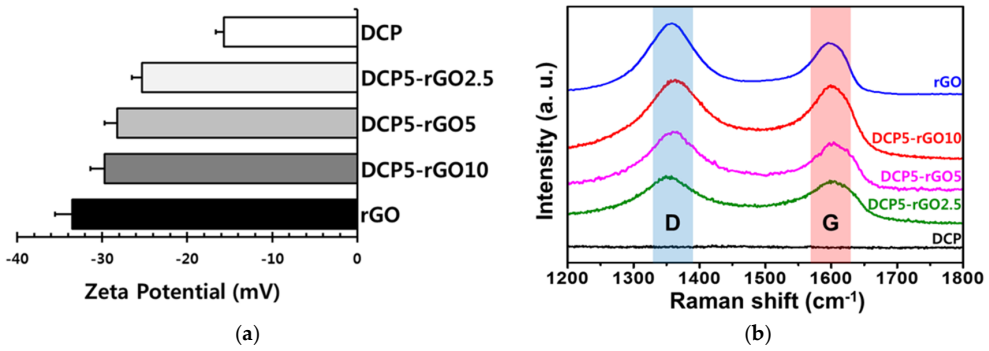

Figure 3. Characterizations of DCP microparticles and DCP-rGO hybrid composites. (**a**) Surface charges and (**b**) Raman spectra of DCP microparticles and DCP-rGO hybrid composites.

To examine the influence of DCP-rGO composites on the growth of MC3T3-E1 cells, their proliferation was assessed, and the results were shown in Figure 4. It has been extensively known that the DCP has an excellent biocompatibility, and can be used in various dental and pharmaceutical fields [66,67]. We also confirmed the biocompatibility of DCP microparticles at a concentration of 5 μg/mL (Figure 4a). On the other hand, the cytotoxicity of rGO has been reported to be strongly dependent on its concentrations [68–70]. Hence, we evaluated the effects of rGO on cell proliferation with increasing concentrations of rGO (2.5–10 μg/mL). There were no significant differences in the proliferation of MC3T3-E1 preosteoblasts between experimental groups, indicating that the rGO at concentrations that were used in the present study have no harmful effects on MC3T3-E1 cells. In addition, the DCP-rGO hybrid composites were also found to be non-cytotoxic to the MC3T3-E1 preosteoblasts (Figure 4b). The proliferation of MC3T3-E1 cells treated with DCP-rGO composites was comparable to that of control group. Meanwhile, the proliferation rates of MC3T3-E1 cells treated with DCP5-rGO2.5 and DCP5-rGO5 composites were decreased at 14 days. In general, the proliferation of various types of cells is retarded when the cells begin to differentiate into specific cell lineages under in vitro conditions [71–73]. We therefore examined the osteogenic differentiation of MC3T3-E1 cells to further investigate the effects of DCP-rGO composites.

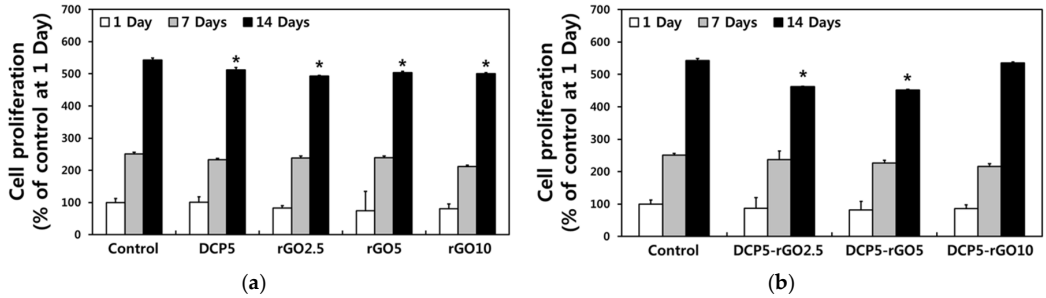

Figure 4. (**a**) Proliferation of MC3T3-E1 cells treated with 5 μg/mL of DCP or 2.5, 5 and 10 μg/mL of rGO. (**b**) Proliferation of MC3T3-E1 cells treated with DCP-rGO hybrid composite. Cultures with fresh media were used as the negative control. An asterisk (*) denotes a significant difference when compared with the control, $p < 0.05$.

The osteogenic differentiation of MC3T3-E1 cells treated with DCP, rGO and DCP-rGO hybrid composites was evaluated by assessing ALP activity and mineralization of calcium. The ALP is a well-established marker for early osteogenesis, and is strongly related to the mineralization ability of osteoblasts [74,75]. Figure 5 showed the ALP activities of cells for 1 to 14 days. As shown in Figure 5a, cells did not show appreciable increase in ALP activity after 14 days of incubation with 5 μg/mL of DCP, 2.5 μg/mL of rGO, and 5 μg/mL of rGO. However, the ALP activity of cells treated with 10 μg/mL of rGO was significantly increased after seven days of incubation. According to the previous studies, rGO can enhance ALP activity and osteogenic differentiation by the distinctive wrinkled features of rGO, which can provide physical stress [76,77]. The DCP also has osteoconductive properties, but the amount of DCP that was used in the present study was insufficient to promote osteogenic differentiation. On the other hand, when the cells were incubated with DCP-rGO composites, the ALP activities were significantly increased regardless of the concentration ratio of DCP to rGO. These findings indicated that the DCP-rGO hybrid composites can effectively increase the ALP activity by the synergistic effects of DCP and rGO. In particular, the MC3T3-E1 cells treated with DCP5-rGO10 composites showed the highest ALP activity as compared with DCP5-rGO2.5 and DCP5-rGO5 groups, suggesting that the concentration ratio of DCP to rGO was a significant factor in facilitating osteogenic differentiation. In addition, these results implied that the decreases in the proliferation rates of MC3T3-E1 cells treated with DCP5-rGO2.5 and DCP5-rGO5 composites could be attributed to the fact that the cells treated with DCP-rGO hybrid composites began to differentiate into osteogenic lineage (Figure 4b). On the other hand, interestingly, the DCP5-rGO10 composites increased the ALP activity without hindering the proliferation rate of cells. Therefore, the DCP5-rGO10 composites might have both biocompatibility and enhancing effects on the osteogenic differentiation.

To further explore the synergistic effects of DCP and rGO, the deposition of calcium phosphate, considered as a marker for bone regeneration, was detected by ARS staining (Figure 6). As presented in Figure 6a, the extracellular calcium deposition stained with ARS (red color) was clearly observed in MC3T3-E1 cells treated with DCP-rGO hybrid composites. To compare the relative amount of calcium deposition, the ARS in stained cells was extracted and quantified (Figure 6b,c). The mineralized nodules were significantly increased in cells that were treated with rGO, and it was especially increased even after seven days of incubation with 10 μg/mL of rGO. These results could be due to the fact that the rGO can effectively adsorb serum proteins in culture media, results in the promoted and accelerated the osteogenic differentiation [77,78]. In addition, the extracellular calcium deposition was further increased when the cells were treated with DCP-rGO hybrid composites, indicating that the DCP and rGO can synergistically increase the osteogenic differentiation of MC3T3-E1 preosteoblasts (Figure 6c). Moreover, the cells treated with DCP5-rGO10 composites showed the highest mineralized nodule among experimental groups, implying that the DCP-rGO composites having DCP and rGO at the concentration ratio of 5:10 μg/mL is the most effective for both early and late osteogenic

differentiation. Therefore, in conclusion, our results suggested that the DCP-rGO hybrid composites can efficiently increase the osteogenic differentiation by the synergistic effects of DCP and rGO, and can be a promising candidate as bone fillers and bone grafts for bone tissue regeneration.

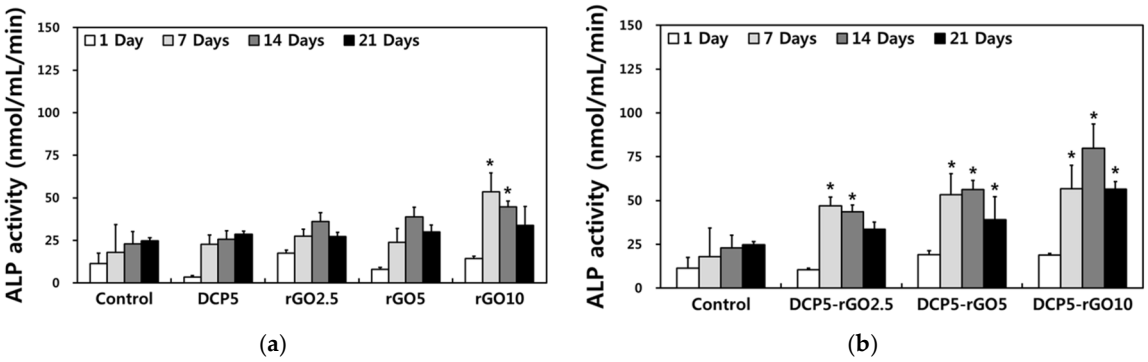

Figure 5. (**a**) ALP activity of MC3T3-E1 cells treated with 5 μg/mL of DCP or 2.5, 5, and 10 μg/mL of rGO. (**b**) ALP activity of MC3T3-E1 cells treated with DCP-rGO hybrid composite. Cultures with fresh media were used as the negative control. An asterisk (*) denotes a significant difference compared with the control, $p < 0.05$.

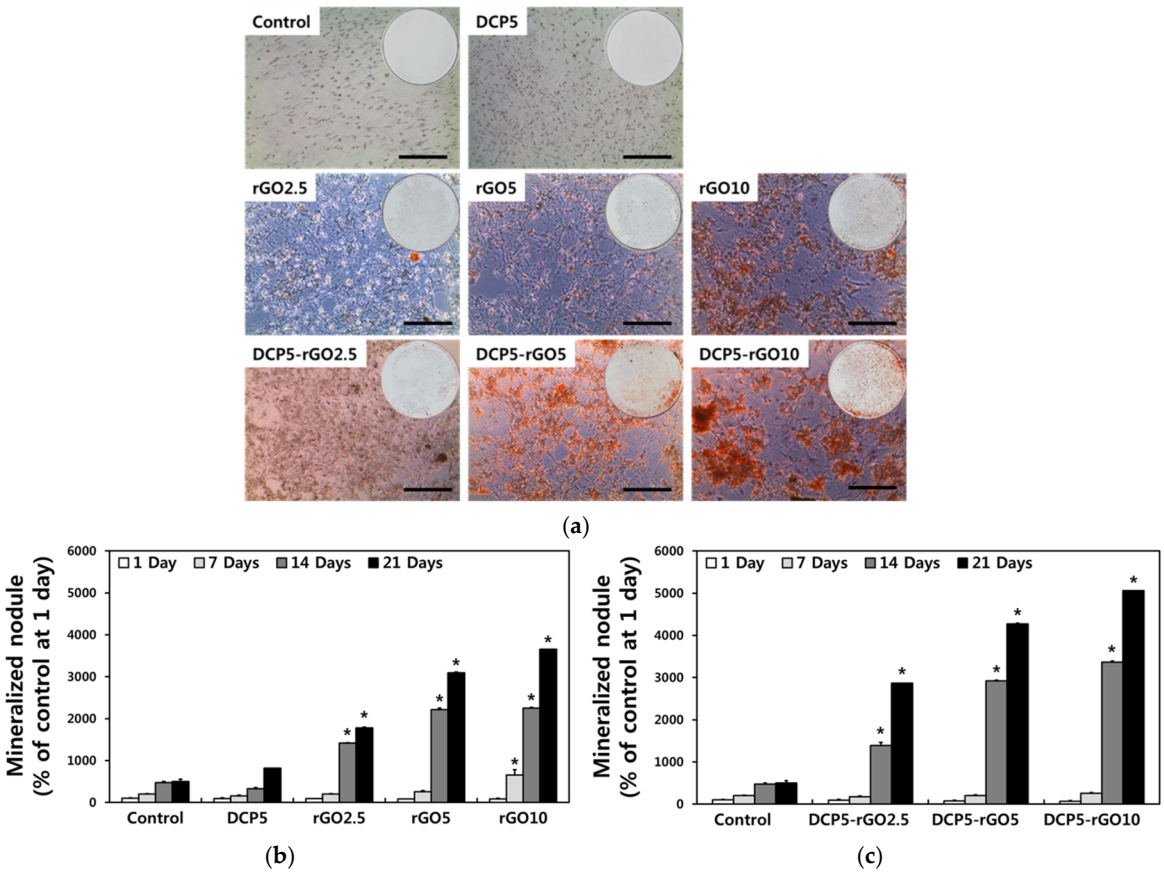

Figure 6. Effects of DCP-rGO hybrid composites on calcium mineralization. (**a**) ARS staining images of MC3T3-E1 cells treated with DCP, rGO, and DCP-rGO hybrid composites. Scale bars are 200 μm. (**b**) Quantification of ARS extracts in MC3T3-E1 cells treated with 5 μg/mL of DCP or 2.5, 5 and 10 μg/mL of rGO. (**c**) Quantification of ARS extracts in MC3T3-E1 cells treated with DCP-rGO hybrid composite. Cultures with fresh media were used as the negative control. An asterisk (*) denotes a significant difference when compared with the control, $p < 0.05$.

4. Conclusions

The aim of this study was to design and develop hybrid composites composed of DCP microparticles and rGO beneficial to osteogenic differentiation for applications to bone tissue engineering. In the present study, we successfully prepared DCP-rGO hybrid composites, and characterized their physicochemical properties. In addition, we demonstrated that the DCP-rGO hybrid composites can be readily formed, and that they are non-toxic to the MC3T3-E1 preosteoblasts. Moreover, our results revealed that the DCP-rGO composites are highly effective for promoting osteogenic differentiation because of the synergistic effects of DCP and rGO. On the other hand, it was found that the concentration ratio of DCP-rGO composites is a significant factor in enhancing osteogenic differentiation of MC3T3-E1 cells, and the composites having DCP and rGO at the concentration ratio of 5:10 μg/mL are quite effective for facilitating osteogenic differentiation. Furthermore, we used commercially available DCP microparticles as a constituent material of composites, and demonstrated that the rGO can be used in a combination with commercially available products. Although many studies have been conducted to explore the potentials of calcium phosphate and rGO composites, our findings clearly suggest that the potentials of DCP-rGO hybrid composites have become more prominent in various industrial fields, as well as research area. In summary, while further comprehensive and systematic studies with the DCP-rGO hybrid composites have to be accomplished before their practical applications, we can reasonably envision the DCP-rGO hybrid composites can be employed as bone substitute materials for bone tissue regeneration and engineering.

Acknowledgments: This research was supported by a grant of the Korea Health Technology R&D Project through the Korea Health Industry Development Institute (KHIDI) funded by the Ministry of Health & Welfare, Republic of Korea (No. HI15C1535), Basic Science Research Program through the National Research Foundation (NRF) of Korea funded by the Ministry of Education (No. 2016R1D1A1B03931076), and the Materials and Components Technology Development Program of MOTIE/KEIT (No. 10052783).

Author Contributions: Dong-Wook Han and Bongju Kim as the principal investigators take the primary responsibility for the paper. Jun Jae Lee, Yong Cheol Shin, Dong-Wook Han, and Bongju Kim conceived and designed the overall experiments. Jun Jae Lee and Yong Cheol Shin prepared the DCP-rGO hybrid composites, contributed in the cell cultures and in vitro assays, and drafted the manuscript. Su-Jin Song and Suck Won Hong carried out the characterizations of DCP-rGO hybrid composites. Young-Jun Lim, Seung Jo Jeong and Jae Min Cha performed the statistical analysis. All authors reviewed this manuscript.

Conflicts of Interest: The authors declare no conflict of interest.

References

1. Qiao, F.; Li, D.; Jin, Z.; Gao, Y.; Zhou, T.; He, J.; Cheng, L. Application of 3D printed customized external fixator in fracture reduction. *Injury* **2015**, *46*, 1150–1155. [CrossRef] [PubMed]
2. Friedlaender, G.E.; Perry, C.R.; Cole, J.D.; Cook, S.D.; Cierny, G.; Muschler, G.F.; Zych, G.A.; Calhoun, J.H.; LaForte, A.J.; Yin, S. Osteogenic protein-1 (bone morphogenetic protein-7) in the treatment of tibial nonunions: A prospective, randomized clinical trial comparing rhOP-1 with fresh bone autograft. *J. Bone Joint Surg. Am.* **2001**, *83*, S151–S158. [CrossRef] [PubMed]
3. Phieffer, L.S.; Goulet, J.A. Delayed unions of the tibia. *J. Bone Joint Surg. Am.* **2006**, *88*, 205–216. [CrossRef]
4. Perren, S.M. Evolution of the internal fixation of long bone fractures: The scientific basis of biological internal fixation: Choosing a new balance between stability and biology. *J. Bone Joint Surg. Br.* **2002**, *84*, 1093–1110. [CrossRef] [PubMed]
5. Kapoor, H.; Agarwal, A.; Dhaon, B.K. Displaced intra-articular fractures of distal radius: A comparative evaluation of results following closed reduction, external fixation and open reduction with internal fixation. *Injury* **2000**, *31*, 75–79. [CrossRef]
6. Damien, C.J.; Parsons, J.R. Bone graft and bone graft substitutes: A review of current technology and applications. *J. Appl. Biomater.* **1991**, *2*, 187–208. [CrossRef] [PubMed]
7. Bauer, T.W.; Muschler, G.F. Bone graft materials: An overview of the basic science. *Clin. Orthop. Rel. Res.* **2000**, *371*, 10–27. [CrossRef]

8. Al Ruhaimi, K.A. Bone graft substitutes: A comparative qualitative histologic review of current osteoconductive grafting materials. *Int. J. Oral Maxillofac. Implants* **2001**, *16*, 105–114. [PubMed]
9. Al-Jabri, T.; Mannan, A.; Giannoudis, P. The use of the free vascularised bone graft for nonunion of the scaphoid: A systematic review. *J. Orthop. Surg. Res.* **2014**, *9*, 21. [CrossRef] [PubMed]
10. Petite, H.; Viateau, V.; Bensaid, W.; Meunier, A.; de Pollak, C.; Bourguignon, M.; Oudina, K.; Sedel, L.; Guillemin, G. Tissue-engineered bone regeneration. *Nat. Biotechnol.* **2000**, *18*, 959–963. [CrossRef] [PubMed]
11. Wei, G.; Ma, P.X. Structure and properties of nano-hydroxyapatite/polymer composite scaffolds for bone tissue engineering. *Biomaterials* **2004**, *25*, 4749–4757. [CrossRef] [PubMed]
12. Kim, S.-S.; Park, M.S.; Jeon, O.; Choi, C.Y.; Kim, B.-S. Poly (lactide-co-glycolide)/hydroxyapatite composite scaffolds for bone tissue engineering. *Biomaterials* **2006**, *27*, 1399–1409. [CrossRef] [PubMed]
13. Fernandez-Yague, M.A.; Abbah, S.A.; McNamara, L.; Zeugolis, D.I.; Pandit, A.; Biggs, M.J. Biomimetic approaches in bone tissue engineering: Integrating biological and physicomechanical strategies. *Adv. Drug Del. Rev.* **2015**, *84*, 1–29. [CrossRef] [PubMed]
14. Wu, S.; Liu, X.; Yeung, K.W.K.; Liu, C.; Yang, X. Biomimetic porous scaffolds for bone tissue engineering. *Mater. Sci. Eng. R* **2014**, *80*, 1–36. [CrossRef]
15. Venkatesan, J.; Bhatnagar, I.; Manivasagan, P.; Kang, K.-H.; Kim, S.-K. Alginate composites for bone tissue engineering: A review. *Int. J. Biol. Macromol.* **2015**, *72*, 269–281. [CrossRef] [PubMed]
16. Peng, S.; Feng, P.; Wu, P.; Huang, W.; Yang, Y.; Guo, W.; Gao, C.; Shuai, C. Graphene oxide as an interface phase between polyetheretherketone and hydroxyapatite for tissue engineering scaffolds. *Sci. Rep.* **2017**, *7*, 46604. [CrossRef] [PubMed]
17. Nie, W.; Peng, C.; Zhou, X.; Chen, L.; Wang, W.; Zhang, Y.; Ma, P.X.; He, C. Three-dimensional porous scaffold by self-assembly of reduced graphene oxide and nano-hydroxyapatite composites for bone tissue engineering. *Carbon* **2017**, *116*, 325–337. [CrossRef]
18. Metsger, D.S.; Driskell, T.D.; Paulsrud, J.R. Tricalcium phosphate ceramic-a resorbable bone implant: Review and current status. *J. Am. Dent. Assoc.* **1982**, *105*, 1035–1038. [CrossRef] [PubMed]
19. Hench, L.L. Bioceramics: From concept to clinic. *J. Am. Ceram. Soc.* **1991**, *74*, 1487–1510. [CrossRef]
20. Daculsi, G. Biphasic calcium phosphate concept applied to artificial bone, implant coating and injectable bone substitute. *Biomaterials* **1998**, *19*, 1473–1478. [CrossRef]
21. Hing, K.A. Bioceramic bone graft substitutes: Influence of porosity and chemistry. *Int. J. Appl. Ceram. Technol.* **2005**, *2*, 184–199. [CrossRef]
22. Johnson, A.J.W.; Herschler, B.A. A review of the mechanical behavior of CaP and CaP/polymer composites for applications in bone replacement and repair. *Acta Biomater.* **2011**, *7*, 16–30. [CrossRef] [PubMed]
23. Rawlings, C.E. Modern bone substitutes with emphasis on calcium phosphate ceramics and osteoinductors. *Neurosurgery* **1993**, *33*, 935–938. [PubMed]
24. Hou, N.Y.; Perinpanayagam, H.; Mozumder, M.S.; Zhu, J. Novel development of biocompatible coatings for bone implants. *Coatings* **2015**, *5*, 737–757. [CrossRef]
25. Hung, K.-Y.; Lai, H.-C.; Feng, H.-P. Characteristics of RF-sputtered thin films of calcium phosphate on titanium dental implants. *Coatings* **2017**, *7*, 126. [CrossRef]
26. HoRikosHi, I.; Takeguchi, N.; Morii, M.; Hayashi, K.E.N. Effect of sorbed or adsorbed water in powdery medicaments on tablet compressibility. *Chem. Pharm. Bull.* **1977**, *25*, 690–694. [CrossRef] [PubMed]
27. Villalba, G.; Liu, Y.; Schroder, H.; Ayres, R.U. Global phosphorus flows in the industrial economy from a production perspective. *J. Ind. Ecol.* **2008**, *12*, 557–569. [CrossRef]
28. Vaithiyalingam, S.R.; Tuliani, P.; Wilber, W.; Reddy, I.K.; Khan, M.A. Formulation and stability evaluation of ketoprofen sustained-release tablets prepared by fluid bed granulation with Carbopol® 971P solution. *Drug Dev. Ind. Pharm.* **2002**, *28*, 1231–1240. [CrossRef] [PubMed]
29. Paßlack, N.; Schmiedchen, B.; Raila, J.; Schweigert, F.J.; Stumpff, F.; Kohn, B.; Neumann, K.; Zentek, J. Impact of increasing dietary calcium levels on calcium excretion and vitamin D metabolites in the blood of healthy adult cats. *PLoS ONE* **2016**, *11*, e0149190. [CrossRef] [PubMed]
30. Gandolfi, M.G.; Zamparini, F.; Degli Esposti, M.; Chiellini, F.; Aparicio, C.; Fava, F.; Fabbri, P.; Taddei, P.; Prati, C. Polylactic acid-based porous scaffolds doped with calcium silicate and dicalcium phosphate dihydrate designed for biomedical application. *Mater. Sci. Eng. C* **2018**, *82*, 163–181. [CrossRef] [PubMed]
31. Gbureck, U.; Hölzel, T.; Klammert, U.; Würzler, K.; Müller, F.A.; Barralet, J.E. Resorbable dicalcium phosphate bone substitutes prepared by 3D powder printing. *Adv. Funct. Mater.* **2007**, *17*, 3940–3945. [CrossRef]

32. Ferna, E.; Gil, F.J.; Ginebra, M.P.; Driessens, F.C.M.; Planell, J.A.; Best, S.M. Calcium phosphate bone cements for clinical applications. Part I: Solution chemistry. *J. Mater. Sci. Mater. Med.* **1999**, *10*, 169–176.
33. Bohner, M. Physical and chemical aspects of calcium phosphates used in spinal surgery. *Eur. Spine J.* **2001**, *10*, S114–S121. [PubMed]
34. Chow, L.C. Solubility of calcium phosphates. In *Octacalcium phosphate*; Chow, L.C., Eanes, E.D., Eds.; Karger Publishers: Basel, Switzerland, 2001; Volume 18, pp. 94–111.
35. Xia, W.; Razi, M.R.M.; Ashley, P.; Neel, E.A.A.; Hofmann, M.P.; Young, A.M. Quantifying effects of interactions between polyacrylic acid and chlorhexidine in dicalcium phosphate–forming cements. *J. Mater. Chem. B* **2014**, *2*, 1673–1680. [CrossRef]
36. Munting, E.; Mirtchi, A.A.; Lemaitre, J. Bone repair of defects filled with a phosphocalcic hydraulic cement: An in vivo study. *J. Mater. Sci. Mater. Med.* **1993**, *4*, 337–344. [CrossRef]
37. Liu, Y.; Dang, Z.; Wang, Y.; Huang, J.; Li, H. Hydroxyapatite/graphene-nanosheet composite coatings deposited by vacuum cold spraying for biomedical applications: Inherited nanostructures and enhanced properties. *Carbon* **2014**, *67*, 250–259. [CrossRef]
38. Shin, Y.C.; Lee, J.H.; Jin, O.S.; Kang, S.H.; Hong, S.W.; Kim, B.; Park, J.-C.; Han, D.-W. Synergistic effects of reduced graphene oxide and hydroxyapatite on osteogenic differentiation of MC3T3-E1 preosteoblasts. *Carbon* **2015**, *95*, 1051–1060. [CrossRef]
39. Novoselov, K.S.; Geim, A.K.; Morozov, S.V.; Jiang, D.; Zhang, Y.; Dubonos, S.V.; Grigorieva, I.V.; Firsov, A.A. Electric field effect in atomically thin carbon films. *Science* **2004**, *306*, 666–669. [CrossRef] [PubMed]
40. Shin, Y.C.; Lee, J.H.; Jin, L.; Kim, M.J.; Kim, Y.J.; Hyun, J.K.; Jung, T.G.; Hong, S.W.; Han, D.W. Stimulated myoblast differentiation on graphene oxide-impregnated PLGA-collagen hybrid fibre matrices. *J. Nanobiotechnol.* **2015**, *13*, 21. [CrossRef] [PubMed]
41. Park, K.O.; Lee, J.H.; Park, J.H.; Shin, Y.C.; Huh, J.B.; Bae, J.-H.; Kang, S.H.; Hong, S.W.; Kim, B.; Yang, D.J. Graphene oxide-coated guided bone regeneration membranes with enhanced osteogenesis: Spectroscopic analysis and animal study. *Appl. Spectrosc. Rev.* **2016**, *51*, 540–551. [CrossRef]
42. Wan, T.-H.; Chiu, Y.-F.; Chen, C.-W.; Hsu, C.-C.; Cheng, I.; Chen, J.-Z. Atmospheric-pressure plasma jet processed Pt-decorated reduced graphene oxides for counter-electrodes of dye-sensitized solar cells. *Coatings* **2016**, *6*, 44. [CrossRef]
43. Nayak, T.R.; Andersen, H.; Makam, V.S.; Khaw, C.; Bae, S.; Xu, X.; Ee, P.-L.R.; Ahn, J.-H.; Hong, B.H.; Pastorin, G. Graphene for controlled and accelerated osteogenic differentiation of human mesenchymal stem cells. *ACS Nano* **2011**, *5*, 4670–4678. [CrossRef] [PubMed]
44. Ku, S.H.; Park, C.B. Myoblast differentiation on graphene oxide. *Biomaterials* **2013**, *34*, 2017–2023. [CrossRef] [PubMed]
45. Lee, W.C.; Lim, C.H.; Su, C.; Loh, K.P.; Lim, C.T. Cell-assembled graphene biocomposite for enhanced chondrogenic differentiation. *Small* **2015**, *11*, 963–969. [CrossRef] [PubMed]
46. Park, S.Y.; Park, J.; Sim, S.H.; Sung, M.G.; Kim, K.S.; Hong, B.H.; Hong, S. Enhanced differentiation of human neural stem cells into neurons on graphene. *Adv. Mater.* **2011**, *23*, H263–H267. [CrossRef] [PubMed]
47. Li, N.; Zhang, Q.; Gao, S.; Song, Q.; Huang, R.; Wang, L.; Liu, L.; Dai, J.; Tang, M.; Cheng, G. Three-dimensional graphene foam as a biocompatible and conductive scaffold for neural stem cells. *Sci. Rep.* **2013**, *3*, 1604. [CrossRef] [PubMed]
48. Shah, S.; Yin, P.T.; Uehara, T.M.; Chueng, S.T.D.; Yang, L.; Lee, K.B. Guiding stem cell differentiation into oligodendrocytes using graphene-nanofiber hybrid scaffolds. *Adv. Mater.* **2014**, *26*, 3673–3680. [CrossRef] [PubMed]
49. Hummers, W.S., Jr.; Offeman, R.E. Preparation of graphitic oxide. *J. Am. Chem. Soc.* **1958**, *80*, 1339. [CrossRef]
50. Lee, J.H.; Shin, Y.C.; Lee, S.-M.; Jin, O.S.; Kang, S.H.; Hong, S.W.; Jeong, C.-M.; Huh, J.B.; Han, D.-W. Enhanced osteogenesis by reduced graphene oxide/hydroxyapatite nanocomposites. *Sci. Rep.* **2015**, *5*, 18833. [CrossRef] [PubMed]
51. Shin, Y.C.; Lee, J.H.; Kim, M.J.; Hong, S.W.; Kim, B.; Hyun, J.K.; Choi, Y.S.; Park, J.-C.; Han, D.-W. Stimulating effect of graphene oxide on myogenesis of C2C12 myoblasts on RGD peptide-decorated PLGA nanofiber matrices. *J. Biol. Eng.* **2015**, *9*, 22. [CrossRef] [PubMed]
52. Li, M.-J.; Liu, C.-M.; Xie, Y.-B.; Cao, H.-B.; Zhao, H.; Zhang, Y. The evolution of surface charge on graphene oxide during the reduction and its application in electroanalysis. *Carbon* **2014**, *66*, 302–311. [CrossRef]

53. Kim, J.-W.; Shin, Y.C.; Lee, J.-J.; Bae, E.-B.; Jeon, Y.-C.; Jeong, C.-M.; Yun, M.-J.; Lee, S.-H.; Han, D.-W.; Huh, J.-B. The effect of reduced graphene oxide-coated biphasic calcium phosphate bone graft material on osteogenesis. *Int. J. Mol. Sci.* **2017**, *18*, 1725. [CrossRef] [PubMed]
54. Li, Y.; Wu, Y. Coassembly of graphene oxide and nanowires for large-area nanowire alignment. *J. Am. Chem. Soc.* **2009**, *131*, 5851–5857. [CrossRef] [PubMed]
55. Yousefi, N.; Gudarzi, M.M.; Zheng, Q.; Aboutalebi, S.H.; Sharif, F.; Kim, J.-K. Self-alignment and high electrical conductivity of ultralarge graphene oxide-polyurethane nanocomposites. *J. Mater. Chem.* **2012**, *22*, 12709–12717. [CrossRef]
56. Szabó, T.; Berkesi, O.; Forgó, P.; Josepovits, K.; Sanakis, Y.; Petridis, D.; Dékány, I. Evolution of surface functional groups in a series of progressively oxidized graphite oxides. *Chem. Mater.* **2006**, *18*, 2740–2749. [CrossRef]
57. Lobo, A.O.; Corat, M.A.F.; Ramos, S.C.; Matsushima, J.T.; Granato, A.E.C.; Pacheco-Soares, C.; Corat, E.J. Fast preparation of hydroxyapatite/superhydrophilic vertically aligned multiwalled carbon nanotube composites for bioactive application. *Langmuir* **2010**, *26*, 18308–18314. [CrossRef] [PubMed]
58. Zanin, H.; Saito, E.; Marciano, F.R.; Ceragioli, H.J.; Granato, A.E.C.; Porcionatto, M.; Lobo, A.O. Fast preparation of nano-hydroxyapatite/superhydrophilic reduced graphene oxide composites for bioactive applications. *J. Mater. Chem. B* **2013**, *1*, 4947–4955. [CrossRef]
59. Shin, Y.C.; Song, S.-J.; Shin, D.-M.; Oh, J.-W.; Hong, S.W.; Choi, Y.S.; Hyon, S.-H.; Han, D.-W. Nanocomposite scaffolds for myogenesis revisited: Functionalization with carbon nanomaterials and spectroscopic analysis. *Appl. Spectrosc. Rev.* **2018**, *53*. [CrossRef]
60. Mendonça, M.C.P.; Soares, E.S.; de Jesus, M.B.; Ceragioli, H.J.; Ferreira, M.S.; Catharino, R.R.; Cruz-Höfling, M.A. Reduced graphene oxide induces transient blood–brain barrier opening: An in vivo study. *J. Nanobiotechnol.* **2015**, *13*, 78. [CrossRef] [PubMed]
61. Merlen, A.; Buijnsters, J.G.; Pardanaud, C. A guide to and review of the use of multiwavelength Raman spectroscopy for characterizing defective aromatic carbon solids: From graphene to amorphous carbons. *Coatings* **2017**, *7*, 153. [CrossRef]
62. Lee, S.C.; Some, S.; Kim, S.W.; Kim, S.J.; Seo, J.; Lee, J.; Lee, T.; Ahn, J.-H.; Choi, H.-J.; Jun, S.C. Efficient direct reduction of graphene oxide by silicon substrate. *Sci. Rep.* **2015**, *5*, 12306. [PubMed]
63. Jiao, L.; Zhang, L.; Wang, X.; Diankov, G.; Dai, H. Narrow graphene nanoribbons from carbon nanotubes. *Nature* **2009**, *458*, 877–880. [CrossRef] [PubMed]
64. Kudin, K.N.; Ozbas, B.; Schniepp, H.C.; Prud'Homme, R.K.; Aksay, I.A.; Car, R. Raman spectra of graphite oxide and functionalized graphene sheets. *Nano Lett.* **2008**, *8*, 36–41. [CrossRef] [PubMed]
65. Tran, D.N.H.; Kabiri, S.; Losic, D. A green approach for the reduction of graphene oxide nanosheets using non-aromatic amino acids. *Carbon* **2014**, *76*, 193–202. [CrossRef]
66. Kim, H.-W.; Georgiou, G.; Knowles, J.C.; Koh, Y.-H.; Kim, H.-E. Calcium phosphates and glass composite coatings on zirconia for enhanced biocompatibility. *Biomaterials* **2004**, *25*, 4203–4213. [CrossRef] [PubMed]
67. Natesan, K.; Shah, W.; Le, H.R.; Tredwin, C. A critical comparison on biocompatibility of different phases of sol–gel derived calcium phosphates as bone graft materials. *J. Biomater. Tissue Eng.* **2015**, *5*, 655–664. [CrossRef]
68. Wojtoniszak, M.; Chen, X.; Kalenczuk, R.J.; Wajda, A.; Łapczuk, J.; Kurzewski, M.; Drozdzik, M.; Chu, P.K.; Borowiak-Palen, E. Synthesis, dispersion, and cytocompatibility of graphene oxide and reduced graphene oxide. *Colloids Surf. B* **2012**, *89*, 79–85. [CrossRef] [PubMed]
69. Akhavan, O.; Ghaderi, E.; Akhavan, A. Size-dependent genotoxicity of graphene nanoplatelets in human stem cells. *Biomaterials* **2012**, *33*, 8017–8025. [CrossRef] [PubMed]
70. Shin, Y.C.; Song, S.-J.; Hong, S.W.; Jeong, S.J.; Chrzanowski, W.; Lee, J.-C.; Han, D.-W. Multifaceted biomedical applications of functional graphene nanomaterials to coated substrates, patterned arrays and hybrid scaffolds. *Nanomaterials* **2017**, *7*, 369. [CrossRef] [PubMed]
71. Mooney, D.; Hansen, L.; Vacanti, J.; Langer, R.; Farmer, S.; Ingber, D. Switching from differentiation to growth in hepatocytes: Control by extracellular matrix. *J. Cell. Physiol.* **1992**, *151*, 497–505. [CrossRef] [PubMed]
72. Liu, H.-C.; Lee, I.C.; Wang, J.-H.; Yang, S.-H.; Young, T.-H. Preparation of PLLA membranes with different morphologies for culture of MG-63 Cells. *Biomaterials* **2004**, *25*, 4047–4056. [CrossRef] [PubMed]

73. Quarles, L.D.; Yohay, D.A.; Lever, L.W.; Caton, R.; Wenstrup, R.J. Distinct proliferative and differentiated stages of murine MC3T3-E1 cells in culture: An in vitro model of osteoblast development. *J. Bone Miner. Res.* **1992**, *7*, 683–692. [CrossRef] [PubMed]
74. Jadlowiec, J.; Koch, H.; Zhang, X.; Campbell, P.G.; Seyedain, M.; Sfeir, C. Phosphophoryn regulates the gene expression and differentiation of NIH3T3, MC3T3-E1, and human mesenchymal stem cells via the integrin/MAPK signaling pathway. *J. Biol. Chem.* **2004**, *279*, 53323–53330. [CrossRef] [PubMed]
75. Yasuda, Y.; Tatematsu, Y.; Fujii, S.; Maeda, H.; Akamine, A.; Torabinejad, M.; Saito, T. Effect of MTAD on the differentiation of osteoblast-like cells. *J. Endod.* **2010**, *36*, 260–263. [CrossRef] [PubMed]
76. Altman, G.; Horan, R.; Martin, I.; Farhadi, J.; Stark, P.; Volloch, V.; Vunjak-Novakovic, G.; Richmond, J.; Kaplan, D.L. Cell differentiation by mechanical stress. *FASEB J.* **2002**, *16*, 270–272. [CrossRef] [PubMed]
77. Akhavan, O.; Ghaderi, E.; Shahsavar, M. Graphene nanogrids for selective and fast osteogenic differentiation of human mesenchymal stem cells. *Carbon* **2013**, *59*, 200–211. [CrossRef]
78. Lee, W.C.; Lim, C.H.Y.; Shi, H.; Tang, L.A.; Wang, Y.; Lim, C.T.; Loh, K.P. Origin of enhanced stem cell growth and differentiation on graphene and graphene oxide. *ACS Nano* **2011**, *5*, 7334–7341. [CrossRef] [PubMed]